The EMBO Journal (2011) 30, 427–438 | © 2011 European Molecular Biology Organization | All Rights Reserved 0261-4189/11
www.embojournal.org

THE EMBO JOURNAL

Structure of Importin13–Ubc9 complex: nuclear import and release of a key regulator of sumoylation

Marlene Grünwald and Fulvia Bono*

Max Planck Institute for Developmental Biology, Tübingen, Germany

Importin13 (Imp13) is an unusual β-karyopherin that is able to both import and export cargoes in and out of the nucleus. In the cytoplasm, Imp13 associates with different cargoes such as Mago-Y14 and Ubc9, and facilitates their import into the nucleus where RanGTP binding promotes the release of the cargo. In this study, we present the 2.8 Å resolution crystal structure of Imp13 in complex with the SUMO E2-conjugating enzyme, Ubc9. The structure shows an uncommon mode of cargo–karyopherin recognition with Ubc9 binding at the N-terminal portion of Imp13, occupying the entire RanGTP-binding site. Comparison of the Imp13–Ubc9 complex with Imp13–Mago-Y14 shows the remarkable plasticity of Imp13, whose conformation changes from a closed ring to an open superhelix when bound to the two different cargoes. The structure also shows that the binding mode is compatible with the sumoylated states of Ubc9. Indeed, we find that Imp13 is able to bind sumoylated Ubc9 *in vitro* and suppresses autosumoylation activity in the complex.

The EMBO Journal (2011) **30,** 427–438. doi:10.1038/emboj.2010.320; Published online 7 December 2010
Subject Categories: membranes & transport; structural biology
Keywords: Importin13; karyopherin; nuclear import; Ubc9–SUMO; X-ray crystallography

Introduction

The regulated transport of molecules through the nuclear pore complexes (NPCs) is a distinctive feature of the eukaryotic cell. The main facilitators of nucleocytoplasmic transport are cargo receptors belonging to the karyopherin-β family (Görlich and Kutay, 1999; Cook *et al*, 2007; Terry *et al*, 2007). Members of this family that transport proteins into the nucleus are called importins. In contrast, exportins facilitate the export of cargoes from the nucleus to the cytosol. Importins and exportins are regulated by RanGTP in opposite ways. In the cell, RanGTP forms a gradient with high levels of RanGTP in the nucleus and low levels in the cytoplasm. Importins associate with a cognate cargo in the cytoplasm and release it in the nucleus on RanGTP binding. Exportins, conversely, bind their cargo in the presence of RanGTP and release it in the cytoplasm when GTP is hydrolyzed to GDP (Cook and Conti, 2010). Two unusual karyopherins, Importin13 (Imp13) and yeast Msn5 (Mingot *et al*, 2001; Yoshida and Blobel, 2001) can function as both import and export receptors. In human cells, Imp13 can export the translation initiation factor eIF1A and import the exon junction complex components Mago-Y14 as well as several transcription factors that contain a histone-fold motif and the E2 SUMO-conjugating enzyme Ubc9 (Mingot *et al*, 2001; Kahle *et al*, 2005; Walker *et al*, 2009).

Recent structural studies have revealed the mechanistic basis for nuclear targeting and release of Mago-Y14 (Bono *et al*, 2010). In complex with Mago-Y14, Imp13 has a closed ring-like conformation, which can be thought of as composed of an N-terminal and a C-terminal arch facing each other. Mago-Y14 binds to the concave surface of the C-terminal arch via a set of evolutionarily conserved residues. This portion of the import factor is the common site for cargo recognition observed in all but one of the importin crystal structures known to date (Cingolani *et al*, 2002; Cook *et al*, 2007).

The complex with RanGTP (i.e., the snapshot of the nuclear state after cargo release) shows that RanGTP binds to the inner concave surface of the N-terminal arch. Although RanGTP and Mago-Y14 occupy different surfaces on the importin, their binding is nevertheless mutually exclusive because of direct steric clashes between the GTPase and the cargo. This is rather different from the mechanism of substrate release observed in importin-β and transportin, wherein an acidic loop at the interface between the N-and C-terminal arches of these karyopherins is the focal point for cargo uptake and release (Cook *et al*, 2007).

While Mago-Y14 is to date the best-studied example of Imp13-mediated transport, little is known of how Imp13 mediates the nuclear import of another evolutionarily conserved cargo, Ubc9. Ubc9 is an essential protein in mammalian cells with a predominantly nuclear localization (Firestein and Feuerstein, 1998; Rodriguez *et al*, 2001; Hayashi *et al*, 2002; Nacerddine *et al*, 2005; Geiss-Friedlander and Melchior, 2007). It is the only SUMO E2-conjugating enzyme and, as such, is a central player in specifying SUMO substrates and catalyzing all SUMO conjugations in the cell (Melchior, 2000; Johnson, 2004). Sumoylation results in the formation of an isopeptide bond between the C-terminal carboxy group of mature SUMO and the ε-amino-group of a lysine residue in the target protein. SUMO attachment occurs in an ATP-dependent reaction wherein SUMO forms a thioester bond with the E1-activating enzyme heterodimer Aos1–Uba2. SUMO is then transferred to the E2-conjugating enzyme Ubc9, again forming a thioester. The reaction is often enhanced by the intervention of E3 ligases (Melchior, 2000; Johnson, 2004). Sumoylation is crucial in a broad range of cellular processes, wherein it acts at the molecular level by altering the protein–protein interaction properties of its targets in a reversible manner (Johnson, 2004; Geiss-Friedlander

*Corresponding author. Department of Biochemistry, Max-Planck-Institute for Developmental Biology, Spemannstraße 35, Tübingen 72076, Germany. Tel.: +49 7071 6011367; Fax: +49 7071 6011353; E-mail: fulvia.bono@tuebingen.mpg.de

Received: 13 August 2010; accepted: 10 November 2010; published online: 7 December 2010

and Melchior, 2007; Makhnevych *et al*, 2009). The structures of Ubc9 in different complexes and sumoylation states have revealed the molecular basis for E2-dependent protein conjugation (Capili and Lima, 2007b; Knipscheer *et al*, 2008; Tang *et al*, 2008; Sekiyama *et al*, 2010)). The specificity of the sumoylation reaction can be regulated at different levels. For example, it has been shown that the mammalian E2-conjugating enzyme Ubc9 is autosumoylated to regulate target discrimination (Hannich *et al*, 2005; Knipscheer *et al*, 2008; Makhnevych *et al*, 2009). To understand the mechanism by which Ubc9 is transported into the nucleus and how the import step fits into the Ubc9 sumoylation pathway, we determined the structure of the complex of Imp13 with Ubc9 and studied how the sumoylation properties of Ubc9 are affected in the import complex.

Results and discussion

Structure determination

Full-length human (Hs) Imp13 and Ubc9 were expressed independently in *Escherichia coli* and purified to homogeneity. The 126 kDa complex was reconstituted by size-exclusion chromatography using an excess of Ubc9 to saturate the complex. The binary complex crystallized in space group $P2_12_12_1$, with one molecule per asymmetric unit. The structure was solved by molecular replacement (MR) using the human Ubc9 structure (PDB ID 1U9A, (Tong *et al*, 1997)) and the human Imp13 structure (PDB ID 2X19, (Bono *et al*, 2010) as search models. A successful MR solution could only be obtained when the Imp13 search model was separated into fragments that could be fitted initially as rigid bodies (see methods). The final model (Figure 1) has been refined to 2.8 Å resolution with an *R*-free of 26.7%, *R*-factor of 22.4% and good stereochemistry (Table I). In the structure, some disordered stretches of residues at the N- and C-termini of Imp13, as well as a long inter-loop between HEAT 14 and 15 (residues 655–673) and a few residues in loops are missing in the final model; the full-length Ubc9 could be modelled. A sample view of the quality of the electron density of the Imp13–Ubc9 interacting surface is shown in Supplementary Figure S1.

Superhelical conformation of Imp13 when bound to Ubc9

Imp13 consists of 20 consecutive HEAT repeats as previously shown (Bono *et al*, 2010) (Figure 1A and B). Briefly, HEAT repeats are 40 amino-acid motifs that typically fold into two α-helices A and B (Andrade *et al*, 2001) and stack against consecutive repeats to form a superhelix. The A helices form the outer surface of the superhelix and the B helices the inner concave surface. Loops link the two helices within (intra-repeat) and between (inter-repeat) HEAT motifs. In Hs Imp13, most of these loops are short, but longer helical insertions are observed in the intra-repeat loop at HEAT 9 and in the inter-repeat loop between HEAT 17 and 18. The repeats pack against each other generally with a clockwise rotation between successive repeats. This rotation is interrupted around HEAT 4 and 10 by counter-clockwise turns that roughly correspond to hinge regions. Further deviations from canonical HEAT repeat arrangements are found at the first repeat that packs almost perpendicularly against HEAT 2 and the last repeat that consists of three parallel α-helices that cap the

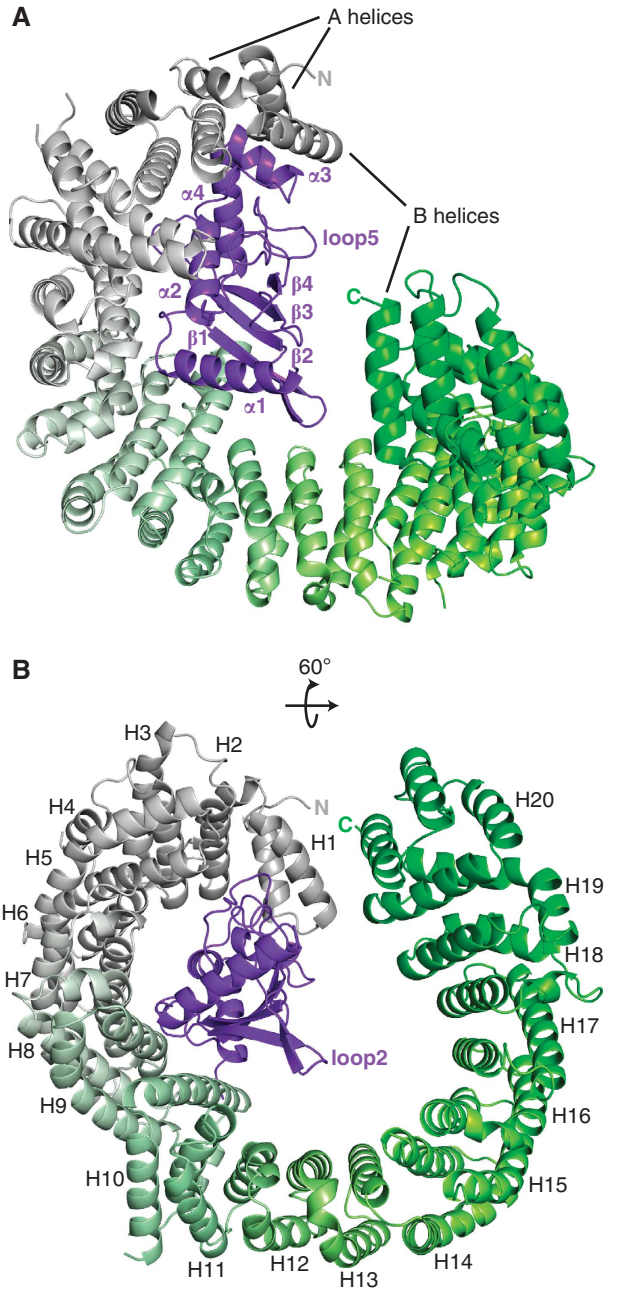

Figure 1 Structure of the Imp13–Ubc9 complex. (**A**) Cartoon view of the complex. Imp13 is shown in green with a colour gradient from grey (N-terminus) to green (C-terminus). Ubc9 is in purple. Secondary structure elements are labelled; (**B**) Cartoon view rotated 60° along the *x* axis. HEAT repeats are labelled from H1 to H20. These and all other protein structure figures were generated using PyMOL (http://www.pymol.org).

superhelix, similar to what was recently observed in the tRNA export receptor, Xpot (Cook *et al*, 2009).

In the Imp13–Ubc9 structure, the HEAT repeats are arranged to form a superhelical structure with the N- and C-terminal ends twisted away from each other. The conformation of Imp13 is, therefore, very different from the ring structure it adopts when in complex with Mago-Y14 (see below). The superhelical pitch extends for ~57 Å with a central hole of ~65–70 Å in diameter (longest diagonal). The C-terminal portion of the molecule is not engaged in

Table I Crystallographic statistics for data collection and refinement

Data collection	
Data set	Imp13–Ubc9
Beamline	SLS PXII
Space group	$P2_12_12_1$
Unit cell (Å)	$a=68.7$, $b=126.8$, $c=184.0$, $\alpha=\beta=\gamma=90^\circ$
Wavelength (Å)	0.9997
Resolution range (Å)[a]	50–2.8 (2.9–2.8)
Unique reflections	40287
Multiplicity	3.7
Completeness (%)[a]	99.4 (99.9)
$I/\sigma(I)$[a]	14.49 (2.37)
R_{sym}(%)[a]	6.9 (67.5)
Refinement	
Resolution range (Å)[a]	50–2.80
R-free (%)[a]	26.7
R-work (%)[a]	22.4
r.m.s.d. Bond (Å)	0.011
r.m.s.d. Angle (deg)	1.4
B factor protein (Å^2)	74.5
Ramachandran values[b]	
Favoured (%)	96.5%
Allowed (%)	99.1%

[a]Values in parentheses correspond to the highest resolution shell.
[b]Molprobity, http://molprobity.biochem.duke.edu/.

binding with the cargo. Ubc9 occupies almost exactly the N-terminal half of the inner surface of the superhelix (Figure 1B).

In the complex with Imp13, Hs Ubc9 shows the canonical E2 catalytic fold that is similar to previously reported structures of the protein in isolation and in other complexes. Ubc9 superimposes with a root mean square deviation (r.m.s.d.) between 0.435 and 1.02 Å (over all Cα atoms) on available Ubc9 structures of the mammalian proteins (Tong *et al*, 1997; Giraud *et al*, 1998; Bernier-Villamor *et al*, 2002; Reverter and Lima, 2005; Yunus and Lima, 2006; Knipscheer *et al*, 2007, 2008; Wang *et al*, 2007; Capili and Lima, 2007a). Ubc9 has an asymmetric structure that contains a four-stranded anti-parallel β-sheet (β1–4) on one side delimited by four α-helices (α1–4) on the other side (Figure 1A). A finer comparison of Ubc9 when in complex with Imp13 and in other structures, detects minor conformational variability in only two loops of Ubc9. The loop between helices α2 and α3 (loop6) is slightly displaced (r.m.s.d. 1.958 Å over 9 Cα atoms) in the Imp13–Ubc9 structure and is engaged in the binding to Imp13. This loop of Ubc9 is also involved in the recognition of the SUMO consensus motif (ΨKXE/D, where Ψ is a bulky hydrophobic residue and X is any residue) for the direct interaction with its substrates (Bernier-Villamor *et al*, 2002) (Supplementary Figure S5). The second part of Ubc9 that deviates from other known structures is a β-hairpin that protrudes from the Ubc9 core domain into the solvent (loop2). The conformation of this loop varies between all Ubc9 structures and so is likely to be intrinsically flexible (Figure 1B).

Extensive interactions mediate Ubc9 recognition by Imp13

Ubc9 fits into the N-terminal arch of Imp13 formed by HEATs 1–9 with direct interactions at two main areas of Imp13 inner surface (Figures 1B, 2A and B). Ubc9 contacts Imp13 mainly through interactions at loop1, loop5 and loop6 (Figure 2A and B and Supplementary Figure S2). A subset of these interacting residues is conserved (Supplementary Figure S2). The first patch of interactions is largely hydrophobic and is facilitated on Ubc9 by loop6 as well as the helix α3 itself, which packs against both helices of HEAT 1 and the B helix of HEAT 2 of Imp13. In particular, Ile125 of Ubc9 ($Ile125_{Ubc9}$) contacts the side chains of Tyr34 of Imp13 ($Tyr34_{Imp}$), $Glu73_{Imp}$ and $Tyr76_{Imp}$ while a second hydrophobic residue, $Tyr134_{Ubc9}$ points towards $Leu33_{Imp}$ and $Tyr34_{Imp}$ (Figure 2A).

The next set of interactions involves HEAT 6–9 of Imp13. Loop1 (the loop between helix α1 and the β-sheet) of Ubc9 packs tightly against HEAT 7, whereas HEAT 7, 8 and 9 of Imp13 are contacted via two positively charged amino acids from the first helix α1 of Ubc9. The interactions on this binding interface are largely polar and involve several positively charged residues contributed by Ubc9. $Arg17_{Ubc9}$ approaches the side chains of $Asp426_{Imp}$ (HEAT 9) and $Leu361_{Imp}$ (HEAT 8), while $Lys18_{Ubc9}$ points towards the residues $Val313_{Imp}$, $Glu317_{Imp}$ and $Asn318_{Imp}$ (HEAT 7). $Thr362_{Imp}$ on HEAT 8 forms polar contacts to both residues of Ubc9. Moreover, two salt bridges are formed between $Asp415_{Imp}$ of HEAT 9 and $Lys59_{Ubc9}$, and between $Glu261_{Imp}$ at HEAT 6 and $Lys110_{Ubc9}$ (Figure 2B).

A smaller set of interactions is formed by loop5 (the β-sheet to α2 loop) of Ubc9 and Imp13 HEAT 4 up to the inter-repeat loop between HEAT 4 and HEAT 5 (Supplementary Figure S2). A closer look reveals that $Asp102_{Ubc9}$ forms a polar interaction with $Thr179_{Imp}$ (at HEAT 4) (Figure 2A).

Thus, the N-terminal arch of Imp13 clamps Ubc9 with specific interactions (Supplementary Figure S2). The Imp13 grasps the Ubc9 as if between an opposing thumb (the N-terminal 2 HEAT repeats) and fingers (the B helices of HEAT repeats 6 to 9) (Figures 1A, B, 2A and B). Consistent with the structural analysis, mutations of both $Tyr34_{Imp}$ and $Tyr35_{Imp}$ to arginine (on the thumb) or of $Asp426_{Imp}$ to arginine (on the fingers) reduced or abolished the binding to Ubc9 in pull-down assays (Figure 2C, lanes 9 and 12 and Supplementary Figure S4C).

Imp13 uses different surfaces to bind Ubc9 and Mago-Y14

The binding mode of Ubc9 to Imp13 is different to that observed with Mago-Y14 and with other karyopherins. The N-terminus of Imp13 shares the highest degree of conservation with the other members of the karyopherin family as it is the binding site for their common regulator, RanGTP (Görlich *et al*, 1997). This is also the region wherein Ubc9 binds. In other importin structures solved to date, cargo molecules are usually found associated with the C-terminal arch of the importin (Cingolani *et al*, 1999; Lee *et al*, 2003, 2006; Cansizoglu *et al*, 2007; Imasaki *et al*, 2007; Wohlwend *et al*, 2007; Mitrousis *et al*, 2008; Bhardwaj and Cingolani, 2010). The only previously observed exception is a cargo of importin-β, the parathyroid hormone-related protein (PTHrP) that binds in an extended conformation at the N-terminal arch between HEAT 2 and 11 (Cingolani *et al*, 2002) (Supplementary Figure S4).

While Ubc9 interaction requires only the N-terminal half of Imp13 (Figures 3D and 4A), Mago-Y14 binding engages HEAT repeats from 5 to the very last helix of HEAT 20. Moreover,

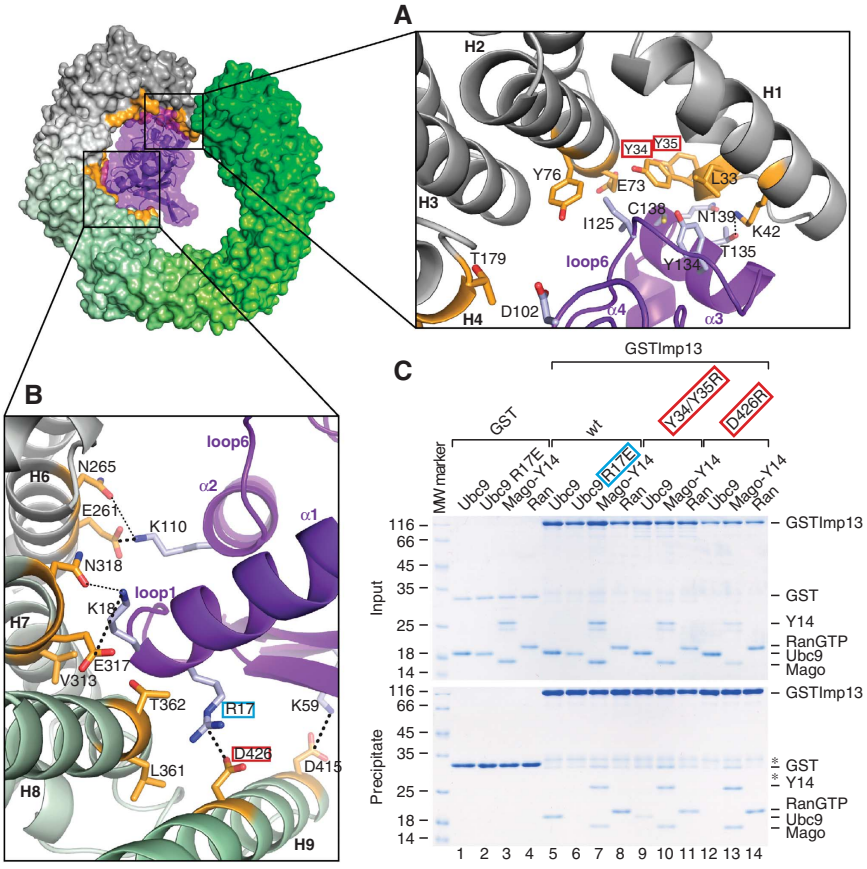

Figure 2 Details of the interactions between Imp13 and Ubc9. (**A**, **B**) show close up views of the interactions between Imp13 and Ubc9. In the upper left, the molecule is rendered as surface in a similar colour code and in a similar orientation as in Figure 1B. Interacting residues on Imp13 are in orange and interacting side-chains on Ubc9 are in pale blue for clarity. The views show the interaction between HEATs 1, 2 and 4 of Imp13 and the loop6 of Ubc9 (**A**), HEATs 7–9 of Imp13 and the loop1 of Ubc9, and between HEAT 6 and the helix α2 of Ubc9 (**B**). Residues of Imp13 and Ubc9 are labelled and HEAT repeats are in black (bold). Secondary structure elements of Ubc9 are labelled in purple. H bonds and charged interactions are shown as regular dotted lines and bold dotted lines, respectively. See also the corresponding electron density in Supplementary Figure S1. Residues mutated in 2C are highlighted with a red (Imp13) or blue (Ubc9) box. (**C**) Protein co-precipitations by GST pull-down assays. GST-tagged Imp13 wild type (wt) or mutant (labelled with a red box) was incubated with Ubc9 wt or mutant (blue box) in a buffer containing 50 mM NaCl. One-sixth of the sample was kept as input control (upper panel) and the rest was co-precipitated with glutathione sepharose beads (lower panel). Both input and pull-down samples were analyzed on Coomassie stained 15% SDS–PAGE. Lanes 1–4 show binding to GST as control. The far left lane was loaded with a molecular weight marker. The gels show some contamination between 35 and 25 KDa (marked with *), probably resulting from degradation of GSTImp13.

the two cargoes bind to the inner surface of Imp13 shifted towards opposite sides: Ubc9 is shifted towards the protruding N-terminal HEAT repeats and at the intra-repeat loops, whereas Mago-Y14 is enclosed by Imp13 on the side of the inter-repeat loops. The conformation of Imp13 in the two complexes is dramatically different (r.m.s.d. 8.4 Å over 792 Cα atoms). In complex with Mago-Y14, Imp13 has an open toroid conformation with the edges of HEAT 1 and HEAT 20 in close proximity (~22 Å distance) while in the complex with Ubc9, the edges of the superhelix are twisted and displaced ~43 Å apart (Figure 3A and C). Ubc9 and Mago-Y14 bind to non-overlapping sites at the inner surface of Imp13. HEAT 8 and HEAT 9 are contacted by both cargoes but at opposite ends of the B helices. While Ubc9 binds towards the tip of the helices of HEAT 4 and 6, Y14 binds adjacently at the following inter-repeat loops (Figure 3, Supplementary Figures S2 and S4). Consistent with these different binding modes, mutations of the human Imp13 corresponding to *Drosophila* mutations that were previously described to impair Mago-Y14 binding (Bono *et al*, 2010) do not affect Ubc9 binding to Imp13 (Figure 3D, lane 7 and Supplementary Figure S4). Moreover, a C-terminally truncated version of Imp13 (Imp13ΔC; HEATs 1–14, residues 1–672) retains its binding ability to Ubc9 and RanGTP (see below) but not to Mago-Y14. Indeed, more than half of Mago-Y14 interaction sites at the C-terminus of Imp13 are missing in the truncated mutant.

Both Ubc9 and Mago-Y14 are nuclear proteins at steady state (Seufert *et al*, 1995; Firestein and Feuerstein, 1998; Kataoka *et al*, 2000; Le Hir *et al*, 2001; Rodriguez *et al*, 2001). Ubc9 can sumoylate targets such as RanGAP in the cytoplasm (Matunis *et al*, 1996; Mahajan *et al*, 1997) and Mago-Y14 shuttles to the cytoplasm as part of the mRNP-associated EJC (Le Hir *et al*, 2001). Given that Ubc9 and Mago-Y14 are both specifically imported by Imp13 and that they sit at opposite sides of Imp13, we asked whether the two cargoes could bind concomitantly to be transported by Imp13 at the same time. A superposition of the two structures does not indicate any obvious steric clashes between the two import cargoes; however, the two structures could not be

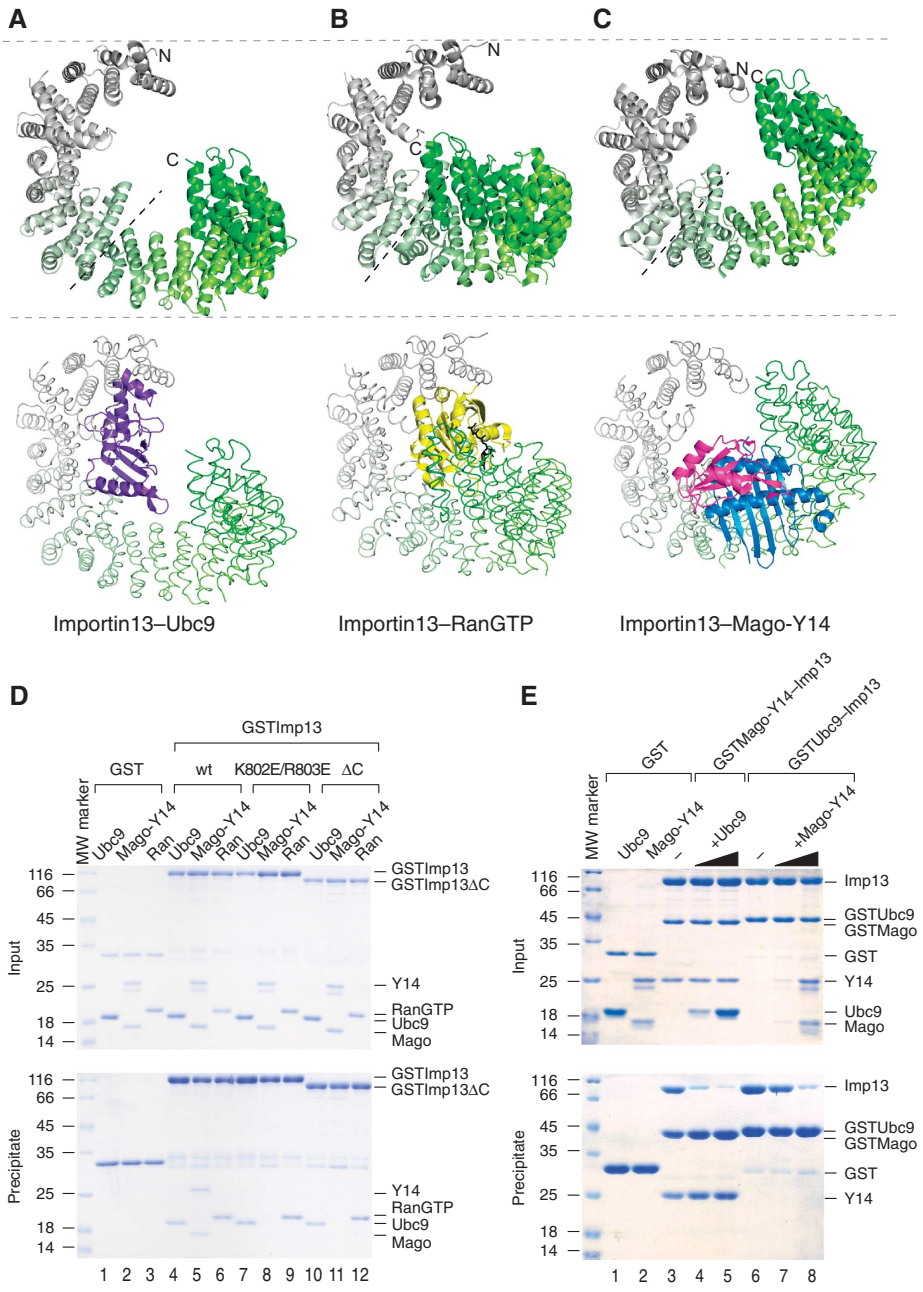

Figure 3 Conformational changes and binding mode of Imp13 in different complexes. (**A**–**C**) Conformational changes of Imp13 bound to (**A**) Ubc9, (**B**) RanGTP and (**C**) Mago-Y14. In the upper panel, the bound molecules are removed for clarity. Imp13 is represented as a cartoon with the same colour coding and view as in Figure 1A. The hinge point at HEAT 10 is represented as a dashed line in black. In the lower panel, Imp13 is represented as a ribbon trace while the bound molecules are shown as a cartoon. Ubc9 is in purple (**A**), Ran in yellow and GTP in black (**B**), Mago in blue, and Y14 in magenta (**C**). (**D**) Protein co-precipitation of GSTImp13 wt, of a GSTImp13 double mutant that was previously shown to impair the binding to Mago-Y14 (Bono *et al*, 2010) and of a GSTImp13 C-terminally truncated mutant (GSTImp13ΔC, H1–14). Both Imp13 K802E/R803E and GSTImp13ΔC mutants retain their ability to bind Ubc9 (lane 7, 10) and RanGTP (lane 9, 12). (**E**) On the left, competition assay of Ubc9 to Imp13–Mago-Y14 and on the right side of Mago-Y14 to Imp13–Ubc9. Both cargoes can displace each other and no concomitant binding is detected. In this competition experiment, 4 μg of GST, GST–Ubc9-Imp13 or GST–Mago-Y14-Imp13 were incubated on beads and competing amounts of Ubc9 (lanes 4 and 5) or of Mago-Y14 (lanes 7 and 8) were added (1 μg and 4 μg lanes 4, 7 and 5, 8, respectively).

optimally aligned because of the large conformational differences. Competition experiments show that increasing amounts of Ubc9 displace Imp13 bound to an immobilized GST fusion of Mago-Y14 (GST–Mago-Y14) and vice versa, clearly indicating that the binding of the two import cargoes is mutually exclusive (Figure 3E). This suggests that the different conformations of the two import complexes prevent mutual binding, allowing only one import cargo to bind at a time.

Mechanism of Ubc9 release from Imp13 by RanGTP

The Imp13–Ubc9 complex forms in the cytosol and translocates through the NPCs into the nucleus. There, on RanGTP binding to Imp13, Ubc9 is dissociated. RanGTP has three main attachment surfaces on Imp13. The first encompasses HEATs 1–4. The second interaction surface is centred at the protruding B helix of HEAT 9, which is in analogous position to the acidic loop at HEAT 8 in other importins. The last

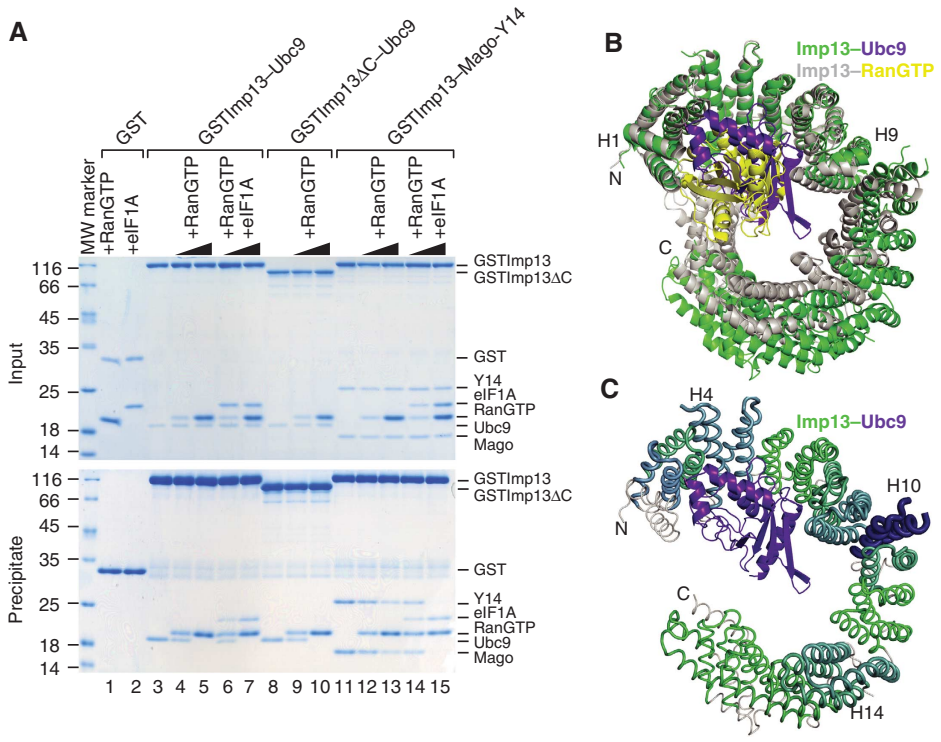

Figure 4 Cargo release by RanGTP. (**A**) Cargo release by increasing amounts of RanGTP (lanes 4, 5, 9, 10, 12, 13) and of RanGTP + eIF1A (lanes 6, 7, 14, 15) is shown in a competition assay on Imp13–Ubc9 (lanes 4–7), Imp13ΔC (HEATs 1–14)–Ubc9 (lanes 9, and 10) and Imp13–Mago-Y14 (lanes 12–15). RanGTP promotes the full dissociation of Ubc9 bound to Imp13ΔC (lane 10). Lanes 1 and 2 show binding of RanGTP and eIF1A to GST as control. (**B**) Superposition of Imp13–Ubc9 and Imp13–RanGTP (PDB ID 2X19). Imp13–Ubc9 is shown in green with a similar view as in Figure 1 after a 180° rotation around the *y* axis, after optimal superposition of the N-termini. Imp13 in complex with RanGTP is shown in grey, Ran is shown in yellow (Supplementary Figure S4C). (**C**) Sausage-like representation of the conformational differences between Imp13 in complex with Ubc9, and Imp13 in complex with RanGTP (calculated according to (Cook *et al*, 2009)). The wider the section of the ribbon and the darker the color, the more variability exists between the two structures. The complex is in the same orientation as in panel 4B. Hinge regions are labelled.

interaction surface involves HEAT 16–19 by which RanGTP bridges the gap between the N-and C-terminal edges of Imp13 (Bono *et al*, 2010). The comparison of the Imp13–Mago-Y14 structure and the Imp13–RanGTP structure shows that a dramatic conformational change takes place on Ran binding, whereupon the Imp13 assumes a more closed conformation. Mago-Y14 and Ran are bound on opposite sides of the molecule and the reverse-charge mutation of $Lys802_{Imp}$ and $Arg803_{Imp}$ to glutamate residues (corresponding to Lys814 and Lys815 in *Drosophila* Imp13) impairs Mago-Y14 binding but not RanGTP or Ubc9 binding (Figure 3D, lanes 7–9 and Supplementary Figure S4).

Surprisingly, Ubc9- and Ran-binding surfaces largely overlap at the N-terminal half of Imp13, with Ubc9 only lacking the C-terminal contact region (Figure 4B). On Imp13, Ubc9 and RanGTP bury a surface area of 1438.6 $Å^2$ and 1567.7 $Å^2$, respectively (as determined by the PISA server; (Krissinel and Henrick, 2007)). Ubc9 and RanGTP interact with Imp13 at several conserved positions on Imp13 but of all the conserved residues at the Ubc9 interface, only two are specific for this cargo (Supplementary Figure S2). Comparison of the Imp13 conformation in the Ubc9-bound complex and in the RanGTP-bound complex shows that the overall conformation of the N-terminal arch is quite similar (r.m.s.d. 1.4 Å over 320 atoms) in the two structures, whereas the C-terminal arch assumes a more open conformation in the Ubc9-bound form (Figure 3A and B). The hinge regions, where more significant movements occur on RanGTP binding, are located at HEAT 4, at HEAT 10 and around HEAT 14 (Figure 4C).

As the Ubc9-interacting surface overlaps with that of RanGTP, cargo release is initiated by direct competition rather than steric hindrance as shown for Mago-Y14 dissociation (Bono, 2010). In the Imp13–Ubc9 complex, the C-terminal binding site of RanGTP is exposed, suggesting that it could nucleate RanGTP association with Imp13. However, RanGTP is able to promote Ubc9 dissociation from Imp13ΔC (Figure 4A, lanes 9–10). Thus, the C-terminal interacting surface of Imp13 is not required as a docking point for Ran to start Ubc9 dissociation. The docking of RanGTP on Imp13–Ubc9, likely occurs at the first HEAT repeat and some flexibility to remove Ubc9 might be needed, possibly around HEAT 4, one of the hinge regions (Figure 4C). Interestingly, efficient Mago-Y14 dissociation *in vitro* requires not only RanGTP but also Imp13 export cargo, eIF1A, while eIF1A alone is not sufficient to promote cargo dissociation (Supplementary Figure S6). These results indicate that release from Imp13 might occur via different mechanisms for Ubc9 and Mago-Y14 or that Mago-Y14 binds with higher affinity to Imp13 than Ubc9, requiring the additive effect of eIF1A to be completely displaced (Figure 4A). This suggests that Mago-Y14 release and subsequent incorporation into the nascent mRNP might only occur efficiently when there is abundant eIF1A in the nucleus and, therefore, could point towards a regulatory role for Imp13 in delivering and releasing the cargoes in the appropriate cellular location.

Accessibility of Ubc9 active sites in the structure

The catalytic groove with the conserved Cys93 and the active site residues $Asn85_{Ubc9}$, $Tyr87_{Ubc9}$ is located between the fourth strand and the second α-helix (loop5) (Bernier-Villamor *et al*, 2002) (Figures 1A and 5A). $Cys93_{Ubc9}$ is the catalytic residue that forms a thioester bond with the C-terminal glycine of SUMO. In the Imp13–Ubc9 complex, loop5 is exposed to solvent and its conformation does not show major changes compared with other Ubc9 structures. As mentioned, loop6 of Ubc9 is involved in the recognition of the SUMO consensus motif present on many SUMO targets. In particular, the consensus motif is recognized by residues $Asp127_{Ubc9}$, $Pro128_{Ubc9}$, $Ala129_{Ubc9}$, $Gln130_{Ubc9}$ and $Ala131_{Ubc9}$ on loop6 (Bernier-Villamor *et al*, 2002), all of which are partially accessible in the complex with Imp13 (Supplementary Figure S5A). The main attachment site of SUMO in autosumoylated Ubc9 is the side chain of $Lys14_{Ubc9}$ in helix α1 (Hannich *et al*, 2005; Knipscheer *et al*, 2008; Makhnevych *et al*, 2009) (Figures 1A and 5A). This residue is disordered in the structure and is not involved in Imp13 recognition.

Functional implication for sumoylation in Ubc9 import

Many proteins are modified by SUMO following extra- and intracellular stimuli. In many instances, regulation of sumoylation can occur at the level of the target through post-translational modification (phosphorylation on proximal residues and/or competing modifications of the acceptor Lys) (reviewed in Geiss-Friedlander and Melchior, 2007). However, it can also be regulated via changes in the activity, abundance or localization of the enzymes involved in the SUMO pathway. As mentioned above, although Ubc9 is the only cellular E2 SUMO-conjugating enzyme, it can also be an acceptor protein for sumoylation. Mammalian Ubc9 sumoylation takes places at a non-canonical consensus site in the α1 helix and it modulates target selection (Figure 5A and B and Supplementary Figure S2). It has been shown that the modification efficiency by SUMO conjugated Ubc9 (Ubc9*SUMO) is reduced in the case of RanGAP and is enhanced in the case of Sp100 (Knipscheer *et al*, 2008). The crystal structure of Ubc9*SUMO confirmed SUMO attachment at $Lys14_{Ubc9}$ and revealed a newly created binding surface involving both Ubc9 and SUMO that provides a rationale for improved Sp100 binding.

Superposition of Ubc9 in complex with Imp13 with Ubc9*SUMO (PDB ID 2VRR, (Knipscheer *et al*, 2008) suggests that binding of the modified cargo to Imp13 could be possible (only minor side chain clashes at HEATs 8 and 10 are visible) (Figure 5A and B). The C-terminal arch of Imp13 is not involved in the binding to Ubc9 and as such, is potentially free to accommodate further molecules. To address this issue, we performed *in vitro* sumoylation reactions in presence of the E1 activating enzyme, the heterodimer Aos1–Uba2 (here Aos–Uba for simplicity), SUMO1 (here SUMO for simplicity) and Ubc9. In these reactions, Ubc9 has the double functionality of the E2 enzyme and the target. We then performed *in vitro* pull-down assays to assess the binding capability of Ubc9*SUMO to immobilized GSTImp13. Western blot analysis shows that Imp13 indeed binds to sumoylated Ubc9 showing that modified Ubc9 could also be an import substrate for Imp13 (Figure 5C).

It has been shown that mutations of $Arg17_{Ubc9}$ and $Lys18_{Ubc9}$ significantly reduce SUMO1 conjugation activity *in vitro* probably because of inefficient SUMO transfer to Ubc9 from the E1 activating enzyme (Tatham *et al*, 2003). The same patch of residues of Ubc9 is involved in the binding of SUMO1 in a non-covalent manner (Knipscheer *et al*, 2007; Capili and Lima, 2007a). Structural analysis of the Imp13–Ubc9 interaction surface shows that these two conserved residues are involved in the binding to Imp13 (Figure 2B and above). A reverse charge mutant at $Arg17Glu_{Ubc9}$ loses the ability to bind Imp13 in pull-down assays (Figure 2C, lane 6), indicating that this catalytically inactive version of Ubc9 cannot be imported into the nucleus by Imp13 and showing that this conserved surface on Ubc9 serves multiple roles (Figure 5D, lane 3).

When in complex with Imp13, Ubc9 is no longer able to catalyze autosumoylation reactions (Figure 5D, lane 4) and the addition of RanGTP partially restores the activity by releasing Ubc9 from Imp13. This implies that full activity of Ubc9 is most likely resumed in the nucleus only after dissociation from Imp13 by RanGTP.

Given that Ubc9 catalytic Cys93, site of thioester attachment, is exposed to solvent in our structure, we asked whether SUMO modified Ubc9 via thioester bond (Ubc9∼SUMO) could also associate with Imp13 and whether Ubc9 in complex with Imp13 could accept SUMO from the E1 (Aos–Uba). We observe formation of Ubc9∼SUMO when Ubc9 is bound to Imp13 (Figure 5E, lane 6) with a similar efficiency to Ubc9 apo (Figure 5E, lane 5). Sensitivity of Ubc9–SUMO to a reducing environment indicates that SUMO is indeed attached via a thioester bond. Precipitation of the same reaction on GST beads shows that Ubc9∼SUMO is stably bound to Imp13. However, we cannot exclude that Ubc9 could be in a dynamic equilibrium with Imp13 and could dissociate to accept the thioester from E1–SUMO to then re-associate to Imp13 after attachment.

As previously mentioned, the active-site residues of Ubc9, essential for E2 activity, are mostly exposed to solvent in the complex with Imp13, suggesting that sumoylation of some sets of targets could still occur. However, all other Ubc9 structures solved to date would sterically clash with Imp13, suggesting that no other Ubc9 complex could associate with Imp13 (Supplementary Figure S3). In particular, structural superposition of Ubc9 in complex with SUMO targets RanGAP and E2-25K with Ubc9 in complex with Imp13 show strong steric clashes at the N-terminal arch of Imp13 (Supplementary Figures S3D, E and S5A) that appear to hamper the docking of these substrates to the appropriate position for the reaction. To clarify this issue, we performed a SUMO conjugation reaction of both these targets with Ubc9 alone or in complex with Imp13 (Figure 5F), according to published protocols (Pichler *et al*, 2002; Knipscheer *et al*, 2009). In the conditions used, we observe the appearance of weak bands at the molecular weight predicted for the sumoylated forms of both targets (lane 3 and 6, E2-25K and RanGAP, respectively), as compared with the controls (lanes 2 and 5). This result could indicate that Ubc9 is partially functional in conjugation as most of its active site is exposed although the binding sites of the substrates on Ubc9 are occluded by Imp13 binding. However, we cannot rule out that undetectable amounts of Ubc9 could dissociate from Imp13 and catalyze the reaction, while most of Ubc9 in complex with Imp13 is not

functional. Indeed, from the structural superposition of Ubc9 in complex with Imp13 and in complex with RanGAP*SUMO, it appears that Imp13 could block interaction with the SUMO consensus motif of the target by partially occluding the recognition site for the hydrophobic residue that precedes the Lys (in this case, a Leu) (Supplementary Figure S5A). This

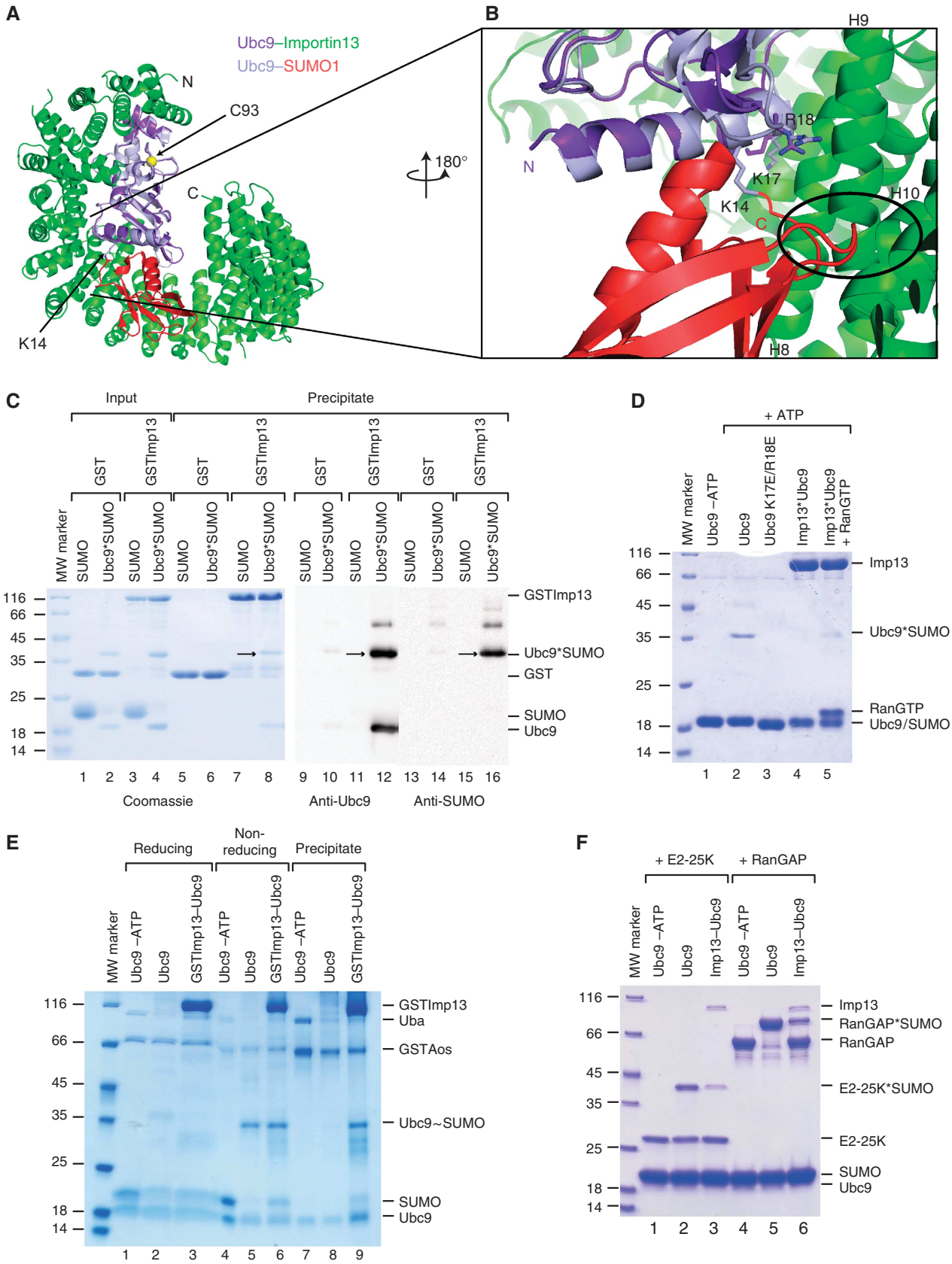

suggests that Imp13 binding could generally interfere with any SUMO consensus motif and supports the hypothesis that the residual activity that we observe in our assay is likely because of dissociation of the Imp13–Ubc9 complex.

Conclusions

We present the structure of Imp13 bound to the import cargo Ubc9. Imp13 has also recently been solved in complex with another import cargo, the Mago-Y14 heterodimer and in its RanGTP-bound nuclear state (Bono *et al*, 2010). Comparison of the three states of Imp13 shows that Imp13 can access a spectrum of conformations, from a tight ring-like structure to a wide, open superhelix.

Ubc9 recognition involves only the N-terminal half of Imp13 and overlaps with the RanGTP-binding surface, showing an unusual mode of binding for an import cargo. The internal surface of the C-terminal arch of Imp13 that provides an extensive cargo-binding surface for Mago-Y14, is not required for the interaction with Ubc9. Although the binding surfaces of the two Imp13 import cargoes mostly differ, concomitant binding is mutually exclusive. Both cargoes can displace each other from Imp13 to a similar extent, suggesting that the discrimination between Ubc9 versus Mago-Y14 in the cytosol perhaps depends on their spatio-temporal abundance and availability.

Binding of RanGTP to Imp13 is required to displace its import cargoes, but it seems that this is achieved through two very different mechanisms. Mago-Y14 is released by a steric hindrance mechanism by RanGTP whereas Ubc9 is released through direct competition for binding at the very N-terminus of Imp13. Interestingly, when Ubc9 dissociation is recapitulated *in vitro,* it works efficiently on RanGTP addition. Conversely, Mago-Y14 release by RanGTP is less efficient and requires the additional presence of Imp13 export cargo, eIF1A, suggesting that the two different modes of binding might also give rise to different requirements for dissociation in the nucleus.

Imp13 binds to two distinct regions on opposite sides of Ubc9, loop1 and 6, through a series of conserved contacts. The interacting surface centred around loop1 is multifunctional and Imp13 binding is not compatible with other known interactions such as non-covalent SUMO binding (Knipscheer *et al*, 2007; Capili and Lima, 2007a) and may also prevent E3 ligase binding (Supplementary Figure S3). Ubc9 is not able to autocatalyze SUMO conjugations when bound to Imp13. This suggests that during import and up to release in the nucleus, Ubc9 is held in a partially inactive state. Conversely, the catalytic cysteine of Ubc9, that mediates the SUMO thioester formation, is not involved in binding Imp13 and is exposed to solvent along with many of the active site residues. Interestingly, Ubc9∼SUMO is also able to associate to Imp13 and Ubc9 can also accept the thioester transfer when in the complex.

A limited number of enzymes function in the sumoylation pathway and target specificity is achieved at different levels in a way that is not fully understood. SUMO modification of the E2 enzyme, Ubc9, can alter substrate specificity (Knipscheer *et al*, 2008). Imp13 is able to associate with both non-modified and covalently modified Ubc9, although the functional significance of this finding is still unclear. Regulated nuclear import of Ubc9 could add yet another level of modulation to the system, tuning the availability of the E2 enzyme in the correct cellular compartment. Indeed it has been shown in mouse germ cells that Ubc9 nuclear localization is dependent on stage-specific Imp13 expression (Yamaguchi *et al*, 2006) and that Imp13 expression in rat and human systems is hormonally and developmentally regulated (Zhang *et al*, 2000). Imp13 might thus provide a molecular link between the cytoplasmic and nuclear function of Ubc9 with a possible regulatory role. Furthermore, the fact that the release of at least some cargoes requires the loading of another cargo points towards another regulatory role of Imp13. In this case, one could envision that efficient transport would occur with abundant cargoes but when some cargoes

Figure 5 Imp13 can bind Ubc9 in different sumoylation states. (**A**) Ubc9 structure superposition of Imp13–Ubc9 and Ubc9*SUMO (PDB ID 2VRR). The view is similar as in Figure 1A. The catalytic cysteine (C93, as a yellow sphere) and the main SUMO-modified lysine (K14) on Ubc9 are labelled. (**B**) Detailed view of the superposition rotated 180° along the *y* axis. Marked with a circle are a loop and the very C-terminal portion of SUMO that might sterically clash with HEAT 8 and 10 of Imp13. K17 and R18 are shown, as well as K14, wherein the C-terminus of SUMO is covalently linked. (**C**) Pull-down analysis of the binding of Ubc9*SUMO to Imp13 (Coomassie stained gel on the left side), revealed by western blot with an anti-Ubc9 (middle panel) and an anti-SUMO antibody (right panel). The arrow indicates the band corresponding to Ubc9*SUMO at the expected molecular weight (lane 8) and specifically detected both by anti-Ubc9 (lane12) and anti-SUMO antibodies (lane 16) (Supplementary Figure S5B). In this experiment, SUMO is His-tagged and, therefore, in the gel shows a molecular weight higher than Ubc9. (**D**) *In vitro* sumoylation reaction in the presence of the purified E1 enzyme, SUMO and Ubc9 (wt or mutated) apo or in complex with Imp13 with or without RanGTP, and ATP. On lane 4, Ubc9 is not modified by SUMO when in complex with Imp13 whereas Ubc9 apo (lane 2) functions as SUMO substrate as shown by the appearance of a band of ∼35 KDa corresponding to Ubc9*SUMO. A K17E/R18E Ubc9 double mutant is catalytically inactive in this condition (lane 3). The same mutant is unable to bind Imp13 (not shown and Figure 2C, lane 6). On lane 1 is the same reaction composition as in lane 2, without ATP as a negative control. (**E**) *In vitro* thioester formation reaction in the presence of the purified E1 enzyme (GSTAos–Uba), SUMO (HisSUMO in this reaction) and Ubc9 apo or in complex with Imp13 with or without ATP and in presence (reducing) or absence (non-reducing) of DTT. Ubc9 is modified by SUMO via formation of the thioester bond both in the apo form (lane 5) and when in complex with Imp13 (lane 6) as shown by the appearance of a band of ∼35 KDa corresponding to Ubc9∼SUMO. A similar reaction in reducing condition does not show the appearance of a band of the same molecular weight, confirming that the band in lanes 5 and 6 corresponds indeed to Ubc9∼SUMO. The three rightmost lanes of the gel correspond to a GST protein co-precipitation of the reactions performed in non-reducing conditions. On lane 9, it is clear that SUMO∼Ubc9 can bind to Imp13. GSTAos also precipitates on the beads but it is not bound to Ubc9 or SUMO∼Ubc9 as judged by the absence of the corresponding bands (lane 8). On lane 1 is the same reaction composition as in lane 2, without ATP and in reducing conditions, while on lanes 4 and 7 is the same reaction composition as in lane 5 and 8, without ATP and in non-reducing conditions as a negative controls. (**F**) SUMO conjugation of Ubc9 substrates E2-25K and RanGAP. The reaction was performed by incubating the purified E1 enzyme, SUMO (HisSUMO in this reaction) and Ubc9 apo or in complex with Imp13 in the presence either of E2-25K (lanes 1–3) or of RanGAP (lanes 4–6). Appearance of a weak band corresponding to SUMO conjugated E2-25K (∼45 KDa) in lane 3 and to RanGAP*SUMO in lane 6, indicates that in presence of Imp13 the reaction is less efficient. In the positive controls, stronger bands appear in presence of Ubc9 apo (lanes 2 and 5). Lanes 1 and 4 are loaded with the same reactions in the absence of ATP as negative controls. On the leftmost lane of all gels the molecular weight markers were loaded.

are depleted, a 'stalled' situation could occur. The absence of one cargo would then also block transport of other cargoes in the opposite direction.

The structure presented here demonstrates that the recognition and release of different cargo proteins by the same molecule can occur with very different mechanisms. Furthermore, we have shown that not only does Imp13 recognize different forms of Ubc9, it can also affect the activity of this cargo. Further structural investigations are needed to understand how Imp13 recognizes other import cargoes and how it promotes export.

Materials and methods

Protein expression and purification

Human Imp13 was expressed in *E. coli* and purified as previously described (Bono *et al*, 2010). Human Ubc9 was cloned in a pETMCN vector, derived from pET Novagen series (C Romier, IGBMC). The protein was expressed as an N-terminal hexahistidine fusion in the *E. coli* strain BL21 (DE3) Gold pLysS (Stratagene) in autoinducing medium (Studier, 2005) at 20°C overnight. Proteins were purified from cleared cell lysates by Ni^{2+} NTA affinity chromatography in buffer A (20 mM Tris (pH 7.5), 300 mM NaCl, 5 mM Imidazole and 1 mM β-mercaptoethanol) with a gradient of 5–250 mM imidazole, followed by proteolytic removal of the affinity tag with the TEV protease during dialysis into buffer B (20 mM Tris (pH 7.5), 100 mM NaCl and 1 mM dithiothreitol (DTT)). After a second pass over the Ni^{2+} NTA column, the collected flow through was further purified by cation-exchange chromatography in buffer B with a gradient of 0.1–1 M NaCl. The human Mago-Y14 full-length was prepared with a similar protocol as previously described, both as an His- or as a GST-tagged complex (Bono *et al*, 2006). Human SUMO1 was cloned in the same pETMCN vector as described for Ubc9. The expression of the protein was carried out in the *E. coli* strain BL21 (DE3) Gold for 3 h at 37°C by induction with 0.5 mM IPTG. The protein was purified by Ni^{2+} NTA affinity chromatography as described for Ubc9, with a further purification by size-exclusion chromatography. pGEX-2TK–Aos1 and pET28a–Uba2 were co-expressed in *E. coli* BL21 (DE3) Gold pLysS at 20°C overnight and purified by Ni^{2+} affinity chromatography as described for Ubc9. A second affinity step on glutathione sepharose beads (Macherey-Nagel) with buffer B was performed and the proteins were eluted with 20 mM reduced glutathione. The purification was completed by a size-exclusion chromatography. For complex formation, proteins were mixed in a 1:1.5 ratio (Imp13/Ubc9 or Imp13/Mago-Y14) in complex buffer (20 mM Tris (pH 7.5), 50 mM NaCl and 1 mM DTT) and incubated on ice for 1 h. The complex was subsequently purified by size-exclusion chromatography (Superdex200 10/300 GL column). Human E2-25K and RanGAP1 were expressed as GST fusion proteins in *E. coli* BL21 DE3 Gold in autoinducing medium at 20°C overnight. The proteins were affinity purified in batch on glutathione sepharose beads with buffer B. After proteolytic cleavage of the GST tag, they were further purified by anion-exchange chromatography followed size-exclusion chromatography as above.

Crystallization, data collection and structure determination

Initial crystals of Imp13–Ubc9 (14 mg/ml) were obtained at 18°C in 50 mM MES (pH 6) and 25% PEG 400 by vapour diffusion. Crystals were optimized by microseeding in 50 mM MES (pH 6.5), 20–25% PEG 300 and grew as needles to a size of $\sim 20 \times 20 \times 200$ μm. They diffracted to 2.8 Å resolution and contained one complex per asymmetric unit. They belong to space group $P2_12_12_1$ with cell dimensions $a = 69$ Å, $b = 127$ Å, $c = 184$ Å, $\alpha = \beta = \gamma = 90°$. Crystallographic data were measured at the PXII beamline at the Swiss Light Source. For data collection, crystals were stabilized in a solution consisting of the mother liquor supplemented with gradually increasing amount of glycerol up to 30% and flash cooled in liquid nitrogen. Data were processed and scaled using XDS (Kabsch, 1993). The structure was solved by MR using PHASER (McCoy *et al*, 2007). The search models included the Imp13 structure (PDB entry 2X19) and Ubc9 structure (PDB entry 1U9A). Owing to the large conformational change in Imp13–Ubc9 compared with the search model, the successful MR solution was only obtained when the Imp13 search model was separated into four fragments encompassing the HEAT repeats ranges H1–H5, H6–H9, H10–H13 and H16–H20 that behaved like rigid bodies. Refinement was carried out using iterative cycles of model building in COOT (Emsley and Cowtan, 2004) and O (Jones *et al*, 1990) and restrained refinement in CNS 1.2 (Brünger *et al*, 1998).

In vitro binding assays

GST-tagged recombinant Imp13, Ubc9 or Mago were mixed with purified binding partners (4 μg of each) in binding buffer (20 mM HEPES (pH 7.5), 50 mM NaCl, 1 mM DTT, 10% glycerol and 0.01% (v/v) Nonidet P40) in a final volume of 60 μl and incubated for 1 h at 4 °C. Attempts to measure the affinity of the interaction between Imp13 and Ubc9 either by surface plasmon resonance (SPR) or by isothermal titration calorimetry (ITC) failed, mainly because a significant percentage of Imp13 aggregates over time (as detected by static light scattering measurement) (data not shown). For the competition experiments, pre-formed complexes were purified by size-exclusion chromatography and 8 μg of complex was mixed with increasing amounts of the competitor proteins. Complexes were immobilized on 15 μl of glutathione agarose beads (Macherey-Nagel) and incubated for 1 h at 4°C. The resin was washed three times with 500 μl of binding buffer and eluted with 10 μl of SDS loading buffer, boiled and loaded on 15% SDS–PAGE with a protein molecular weight marker. Proteins were visualized by Coomassie staining.

In vitro sumoylation assays and western blot analysis

The Ubc9 *in vitro* modification assay was performed essentially as described by Knipscheer *et al*, 2008. For small-scale experiments, 38.5 μg Ubc9 or 270 μg of Imp13–Ubc9 ± 38 μg RanGTP, 1.6 μg Aos1–Uba2 and 7.6 μg SUMO1 (in this paper, SUMO for simplicity) were used in a final volume of 50 μl. The reaction was started by adding 5 mM ATP and incubated for 5 h at 37°C. Large-scale reactions were performed increasing the above components by ~570 folds in the same conditions, before purification. Ubc9*SUMO was purified on an anion-exchange column in buffer C (20 mM Tris (pH 7.5), 100 mM NaCl, 1 mM DTT and 0.1 mM AEBSF) and eluted with a salt gradient of 0.1–1M NaCl, followed by size-exclusion chromatography. After *in vitro* binding assays, the samples were separated by SDS–PAGE and transferred on a nitrocellulose membrane (Whatman). Immunoblotting was performed with mouse anti-SUMO (Zymed, 33–2400, dilution 1:3500) and goat anti-Ubc9 (Abcam, ab21193, dilution 1:3500). Western blots were developed using ECL Plus Western Blotting Detection System (GE Healthcare).

The thioester formation assay was done according to Pichler *et al*, 2002. In the reaction, 2 μg Aos1–Uba2, 1.2 μg SUMO and either 1.2 μg Ubc9 apo or 12 μg of pre-formed GSTImp13–Ubc9 complex and 5 mM ATP were incubated in a total volume of 60 μl for 3 h at 30°C. Of each reaction, 10 μl was treated with reducing buffer and 10 μl with non-reducing loading buffer. The *in vitro* binding assay was performed as described above in non-reducing condition. The remaining of the reaction was immobilized on 20 μl glutathione agarose beads (Macherey-Nagel) for 45 min at 4°C. *In vitro* sumoylation of E2-25K and RanGAP1 was performed as described by Knipscheer *et al*, 2009 in a total volume of 50 μl. The reactions were done with 2 μM Ubc9 or 2 μM pre-formed Imp13–Ubc9 complex respectively. To avoid unspecific binding, in case of RanGAP1, 2 μg BSA was added. The samples were loaded on a SDS–PAGE (Any kD Mini-PROTEAN TGX Precast Gel, BIORAD).

Accession numbers

The coordinates and structure factors have been deposited in the Macromolecular Structure Database of the European Bioinformatic Institute (EBI) with ID code 2xwu.

Supplementary data

Supplementary data are available at *The EMBO Journal* Online (http://www.embojournal.org).

Acknowledgements

We wish to thank Guido Sauer for mass spectrometry analysis and for the SUMO clone, Jerome Basquin, Karina Valer Saldana and Sabine Pleyer at the MPI-Martinsried crystallization facility and

Claire Basquin for biophysical measurements (MPI-Martinsried). We also thank Dirk Görlich (MPI, Goettingen) for the Human Ubc9 clone, Stefan Müller (MPI, Martinsried) for the E1 clones and the staff of the PX beamlines at the Swiss Light Source (Villigen, Switzerland) for assistance during data collection. We thank Oliver Weichenrieder for help with data collection and discussion. We thank Atlanta Cook, Gretel Buchwald, Elisa Izaurralde and Elena Conti for discussion and critical reading of the paper and Thomas Holder and Aleksandar Basara for help with some figures. This study was supported by the Max Planck Gesellshaft and by the DFG grant BO3588/1-1.

Conflict of interest

The authors declare that they have no conflict of interest.

References

Andrade MA, Petosa C, O'Donoghue SI, Müller CW, Bork P (2001) Comparison of ARM and HEAT protein repeats. *J Mol Biol* **309:** 1–18

Bernier-Villamor V, Sampson DA, Matunis MJ, Lima CD (2002) Structural basis for E2-mediated SUMO conjugation revealed by a complex between ubiquitin-conjugating enzyme Ubc9 and RanGAP1. *Cell* **108:** 345–356

Bhardwaj A, Cingolani G (2010) Conformational selection in the recognition of the snurportin importin beta binding domain by importin beta. *Biochemistry* **49:** 5042–5047

Bono F, Cook AG, Grunwald M, Ebert J, Conti E (2010) Nuclear import mechanism of the EJC component Mago-Y14 revealed by structural studies of Importin 13. *Mol Cell* **37:** 211–222

Bono F, Ebert J, Lorentzen E, Conti E (2006) The crystal structure of the exon junction complex reveals how it maintains a stable grip on mRNA. *Cell* **126:** 713–725

Brünger AT, Adams PD, Clore GM, DeLano WL, Gros P, Grosse-Kunstleve RW, Jiang JS, Kuszewski J, Nilges M, Pannu NS, Read RJ, Rice LM, Simonson T, Warren GL (1998) Crystallography & NMR system: a new software suite for macromolecular structure determination. *Acta Crystallogr D Biol Crystallogr* **54:** 905–921

Cansizoglu AE, Lee BJ, Zhang ZC, Fontoura BMA, Chook YM (2007) Structure-based design of a pathway-specific nuclear import inhibitor. *Nat Struct Mol Biol* **14:** 452–454

Capili AD, Lima CD (2007a) Structure and analysis of a complex between SUMO and Ubc9 illustrates features of a conserved E2-Ubl interaction. *J Mol Biol* **369:** 608–618

Capili AD, Lima CD (2007b) Taking it step by step: mechanistic insights from structural studies of ubiquitin/ubiquitin-like protein modification pathways. *Curr Opin Struct Biol* **17:** 726–735

Cingolani G, Bednenko J, Gillespie MT, Gerace L (2002) Molecular basis for the recognition of a nonclassical nuclear localization signal by importin beta. *Mol Cell* **10:** 1345–1353

Cingolani G, Petosa C, Weis K, Müller CW (1999) Structure of importin-beta bound to the IBB domain of importin-alpha. *Nature* **399:** 221–229

Cook A, Bono F, Jinek M, Conti E (2007) Structural biology of nucleocytoplasmic transport. *Annu Rev Biochem* **76:** 647–671

Cook AG, Conti E (2010) Nuclear export complexes in the frame. *Curr Opin Struct Biol* **20:** 247–252

Cook AG, Fukuhara N, Jinek M, Conti E (2009) Structures of the tRNA export factor in the nuclear and cytosolic states. *Nature* **461:** 60–65

Emsley P, Cowtan K (2004) Coot: model-building tools for molecular graphics. *Acta Crystallogr D Biol Crystallogr* **60:** 2126–2132

Firestein R, Feuerstein N (1998) Association of activating transcription factor 2 (ATF2) with the ubiquitin-conjugating enzyme hUBC9. Implication of the ubiquitin/proteasome pathway in regulation of ATF2 in T cells. *J Biol Chem* **273:** 5892–5902

Geiss-Friedlander R, Melchior F (2007) Concepts in sumoylation: a decade on. *Nat Rev Mol Cell Biol* **8:** 947

Giraud MF, Desterro JM, Naismith JH (1998) Structure of ubiquitin-conjugating enzyme 9 displays significant differences with other ubiquitin-conjugating enzymes which may reflect its specificity for sumo rather than ubiquitin. *Acta Crystallogr D Biol Crystallogr* **54:** 891–898

Görlich D, Dabrowski M, Bischoff FR, Kutay U, Bork P, Hartmann E, Prehn S, Izaurralde E (1997) A novel class of RanGTP binding proteins. *J Cell Biol* **138:** 65–80

Görlich D, Kutay U (1999) Transport between the cell nucleus and the cytoplasm. *Annu Rev Cell Dev Biol* **15:** 607–660

Hannich JT, Lewis A, Kroetz MB, Li S-J, Heide H, Emili A, Hochstrasser M (2005) Defining the SUMO-modified proteome by multiple approaches in Saccharomyces cerevisiae. *J Biol Chem* **280:** 4102–4110

Hayashi T, Seki M, Maeda D, Wang W, Kawabe Y-i, Seki T, Saitoh H, Fukagawa T, Yagi H, Enomoto T (2002) Ubc9 is essential for viability of higher eukaryotic cells. *Exp Cell Res* **280:** 212–221

Imasaki T, Shimizu T, Hashimoto H, Hidaka Y, Kose S, Imamoto N, Yamada M, Sato M (2007) Structural basis for substrate recognition and dissociation by human transportin 1. *Mol Cell* **28:** 57–67

Johnson ES (2004) Protein modification by SUMO. *Annu Rev Biochem* **73:** 355–382

Jones TA, Bergdoll M, Kjeldgaard M (eds) (1990) *O: A Macromolecular Modeling Environment*. Springer-Verlag Press, pp 189–195

Kabsch W (1993) Automatic processing of rotation diffraction data from crystals of initially unknown symmetry and cell constants. *J Appl Cryst* **26:** 795–800

Kahle J, Baake M, Doenecke D, Albig W (2005) Subunits of the heterotrimeric transcription factor NF-Y are imported into the nucleus by distinct pathways involving importin beta and importin 13. *Mol Cell Biol* **25:** 5339–5354

Kataoka N, Yong J, Kim VN, Velazquez F, Perkinson RA, Wang F, Dreyfuss G (2000) Pre-mRNA splicing imprints mRNA in the nucleus with a novel RNA-binding protein that persists in the cytoplasm. *Mol Cell* **6:** 673–682

Knipscheer P, Flotho A, Klug H, Olsen JV, van Dijk WJ, Fish A, Johnson ES, Mann M, Sixma TK, Pichler A (2008) Ubc9 sumoylation regulates SUMO target discrimination. *Mol Cell* **31:** 371–382

Knipscheer P, Klug H, Sixma TK, Pichler A (2009) Preparation of sumoylated substrates for biochemical analysis. *Methods Mol Biol* **497:** 201–210

Knipscheer P, van Dijk WJ, Olsen JV, Mann M, Sixma TK (2007) Noncovalent interaction between Ubc9 and SUMO promotes SUMO chain formation. *EMBO J* **26:** 2797–2807

Krissinel E, Henrick K (2007) Inference of macromolecular assemblies from crystalline state. *J Mol Biol* **372:** 774–797

Le Hir H, Gatfield D, Braun IC, Forler D, Izaurralde E (2001) The protein Mago provides a link between splicing and mRNA localization. *EMBO Rep* **2:** 1119–1124

Lee BJ, Cansizoglu AE, Süel KE, Louis TH, Zhang Z, Chook YM (2006) Rules for nuclear localization sequence recognition by karyopherin beta 2. *Cell* **126:** 543–558

Lee SJ, Sekimoto T, Yamashita E, Nagoshi E, Nakagawa A, Imamoto N, Yoshimura M, Sakai H, Chong KT, Tsukihara T, Yoneda Y (2003) The structure of importin-beta bound to SREBP-2: nuclear import of a transcription factor. *Science* **302:** 1571–1575

Mahajan R, Delphin C, Guan T, Gerace L, Melchior F (1997) A small ubiquitin-related polypeptide involved in targeting RanGAP1 to nuclear pore complex protein RanBP2. *Cell* **88:** 97–107

Makhnevych T, Sydorskyy Y, Xin X, Srikumar T, Vizeacoumar FJ, Jeram SM, Li Z, Bahr S, Andrews BJ, Boone C, Raught B (2009) Global map of SUMO function revealed by protein-protein interaction and genetic networks. *Mol Cell* **33:** 124–135

Matunis MJ, Coutavas E, Blobel G (1996) A novel ubiquitin-like modification modulates the partitioning of the Ran-GTPase-activating protein RanGAP1 between the cytosol and the nuclear pore complex. *J Cell Biol* **135:** 1457–1470

McCoy A, Grosse-Kunstleve R, Adams P, Winn M, Storoni L, Read R (2007) Phaser crystallographic software. *J appl crystallogr* **40:** 658–674

Melchior F (2000) SUMO—nonclassical ubiquitin. *Annu Rev Cell Dev Biol* **16:** 591–626

Mingot JM, Kostka S, Kraft R, Hartmann E, Görlich D (2001) Importin 13: a novel mediator of nuclear import and export. *EMBO J* **20:** 3685–3694

Mitrousis G, Olia AS, Walker-Kopp N, Cingolani G (2008) Molecular basis for the recognition of snurportin 1 by importin beta. *J Biol Chem* **283:** 7877–7884

Nacerddine K, Lehembre F, Bhaumik M, Artus J, Cohen-Tannoudji M, Babinet C, Pandolfi PP, Dejean A (2005) The SUMO pathway is essential for nuclear integrity and chromosome segregation in mice. *Dev Cell* **9:** 769–779

Pichler A, Gast A, Seeler JS, Dejean A, Melchior F (2002) The nucleoporin RanBP2 has SUMO1 E3 ligase activity. *Cell* **108:** 109–120

Reverter D, Lima CD (2005) Insights into E3 ligase activity revealed by a SUMO-RanGAP1-Ubc9-Nup358 complex. *Nature* **435:** 687–692

Rodriguez MS, Dargemont C, Hay RT (2001) SUMO-1 conjugation *in vivo* requires both a consensus modification motif and nuclear targeting. *J Biol Chem* **276:** 12654–12659

Sekiyama N, Arita K, Ikeda Y, Hashiguchi K, Ariyoshi M, Tochio H, Saitoh H, Shirakawa M (2010) Structural basis for regulation of poly-SUMO chain by a SUMO-like domain of Nip45. *Proteins* **78:** 1491–1502

Seufert W, Futcher B, Jentsch S (1995) Role of a ubiquitin-conjugating enzyme in degradation of S- and M-phase cyclins. *Nature* **373:** 78–81

Tang Z, Hecker CM, Scheschonka A, Betz H (2008) Protein interactions in the sumoylation cascade: lessons from X-ray structures. *FEBS J* **275:** 3003–3015

Tatham MH, Kim S, Yu B, Jaffray E, Song J, Zheng J, Rodriguez MS, Hay RT, Chen Y (2003) Role of an N-terminal site of Ubc9 in SUMO-1, -2, and -3 binding and conjugation. *Biochemistry* **42:** 9959–9969

Terry LJ, Shows EB, Wente SR (2007) Crossing the nuclear envelope: hierarchical regulation of nucleocytoplasmic transport. *Science* **318:** 1412–1416

Tong H, Hateboer G, Perrakis A, Bernards R, Sixma TK (1997) Crystal structure of murine/human Ubc9 provides insight into the variability of the ubiquitin-conjugating system. *J Biol Chem* **272:** 21381–21387

Walker P, Doenecke D, Kahle J (2009) Importin 13 mediates nuclear import of histone fold containing chrac heterodimers. *J Biol Chem* **284:** 11652–11662

Wang J, Hu W, Cai S, Lee B, Song J, Chen Y (2007) The intrinsic affinity between E2 and the Cys domain of E1 in ubiquitin-like modifications. *Mol Cell* **27:** 228–237

Wohlwend D, Strasser A, Dickmanns A, Ficner R (2007) Structural basis for RanGTP independent entry of spliceosomal U snRNPs into the nucleus. *J Mol Biol* **374:** 1129–1138

Yamaguchi YL, Tanaka SS, Yasuda K, Matsui Y, Tam PPL (2006) Stage-specific Importin13 activity influences meiosis of germ cells in the mouse. *Dev Biol* **297:** 350–360

Yoshida K, Blobel G (2001) The karyopherin Kap142p/Msn5p mediates nuclear import and nuclear export of different cargo proteins. *J Cell Biol* **152:** 729–740

Yunus AA, Lima CD (2006) Lysine activation and functional analysis of E2-mediated conjugation in the SUMO pathway. *Nat Struct Mol Biol* **13:** 491–499

Zhang C, Sweezey NB, Gagnon S, Muskat B, Koehler D, Post M, Kaplan F (2000) A novel karyopherin-beta homolog is developmentally and hormonally regulated in fetal lung. *Am J Respir Cell Mol Biol* **22:** 451–459

